

## Letter to the Editor

# Unveiling the nature of the Cloverleaf lens-system: HST/NICMOS-2 observations<sup>\*</sup>

J.-P. Kneib<sup>1</sup>, D. Alloin<sup>2</sup>, and R. Pelló<sup>1</sup>

<sup>1</sup> Observatoire Midi-Pyrénées, CNRS-UMR5572, 14 Av. Edouard Belin, F-31400 Toulouse, France

<sup>2</sup> CNRS-URA2052, Service d'Astrophysique, CE Saclay, l'Orme des Merisiers, F-91191 Gif-sur-Yvette Cedex, France

Received 17 April 1998 / Accepted 18 October 1998

**Abstract.** We present new elements in the identification of the Cloverleaf lens-system based on recent NICMOS-2/F160W observations. After a careful PSF subtraction of the 4 images of the quasar, the residual  $H_{F160W}$  image reveals the presence of a faint object ( $H \sim 20.5$ ) amid the 4 quasars. This object corresponds to a single galaxy that we identify as the primary lens of the lens-system. From the R, I and H photometry of the galaxies surrounding the Cloverleaf we also derive a photometric redshift. We find that most of them are consistent with belonging to a galaxy cluster/group with mean redshift  $\bar{z} = 0.9 \pm 0.1$ : they are likely to be the other component in the lens-system that provides the additional “external” shear. Furthermore, we detect 2 very red objects (I-H $\sim$ 4): the faintest one has no observed optical ( $R_{F702W}$  and  $I_{F814W}$ ) counterpart, and the brightest has a predicted redshift  $z \sim 2$ , and may be identified with one of the Cloverleaf absorbers. This gravitational-lens system constitutes an excellent target for imaging/spectroscopy with the new generation of 8m ground-based telescopes.

**Key words:** gravitational lensing – clusters of galaxies – gravitational lensing: Cloverleaf (H1413+117)

## 1. Introduction

The excellent quality and broad wavelength coverage of current observations of gravitational-lens systems have allowed to unveil part of their mysteries. The primary lens is often detected. The immediate surrounding of the multiply lensed quasars/galaxies is studied in great detail and generally shows some galaxy clustering (e.g. Tonry 1998, Hjorth & Kneib 1998) or even sometimes X-ray cluster emission (Hattori et al. 1997,

Chartas et al. 1998). Furthermore, the measurement of time-delays (Kundic et al. 1997, Schechter et al. 1997) has strengthened the interest of a detailed study of these gravitational-lens systems in order to use them as a cosmological tool.

Since the identification by Magain et al. (1988) of the gravitational-lens system called the Cloverleaf, made of 4 images of the BAL quasar H1413+117 at  $z=2.558$ , many efforts have been dedicated to a direct search for its lens-system. Early models of the lens have involved one or two galaxy-lenses very close to the line-of-sight toward the quasar (Kayser et al. 1990). A more recent analysis showed that an external shear was needed to correctly model this system (Keeton, Kochanek & Seljak 1997), and indeed it is probably related to the existence of an overdensity of galaxies nearby, as detected by Kneib et al. (1998). The lensing geometry, amplification and time-delays are sensitive to mass distribution of the galaxy-lens expected to be located amid the 4 images of the quasar. A positive detection of the galaxy-lens would bring stringent constraints in the lens modeling. However, despite relatively deep searches: R and I imaging with the HST (Turnshek et al. 1997; Kneib et al. 1998) and K imaging with the Keck telescope (Lawrence et al. 1996), the galaxy-lens has not been detected yet. The galaxy cluster recently revealed near the Cloverleaf (Kneib et al. 1998) was assumed to be at  $z \sim 1.7$  as this corresponds to the mean value of the narrow absorption line-systems observed in the quasar spectra ( $z=1.44, 1.66, 1.87, 2.07$  and  $2.09$ : Turnshek et al. 1988; Magain et al. 1988, Monier et al. 1998). Combining IR data with the  $R_{F702W}$  and  $I_{F814W}$  WFPC-2 data of this system will allow to estimate a likely redshift for the faint galaxies surrounding the Cloverleaf. The recent NICMOS-2/F160W observation consists of a unique dataset to help answer both the existence of the galaxy-lens and to constrain the distance of the surrounding galaxies.

The NICMOS-2 data are presented in Sect. 2, while in Sect. 3 we discuss the identification of the galaxy-lens after the PSF subtraction of the 4 quasar images. The photometric redshifts of the surrounding galaxies are derived in Sect. 4. The discussion and concluding remarks are provided in Sect. 5. Throughout this paper we use  $H_0 = 50$  km/s/Mpc and  $\Omega_0 = 1$ .

Send offprint requests to: D. Alloin (alloin@eso.org)

<sup>\*</sup> Based on observations obtained with the NASA/ESA Hubble Space Telescope, obtained from the data archive at the Space Telescope Science Institute. STScI is operated by the Association of Universities for Research in Astronomy, Inc. under the NASA contract NAS 5-26555.

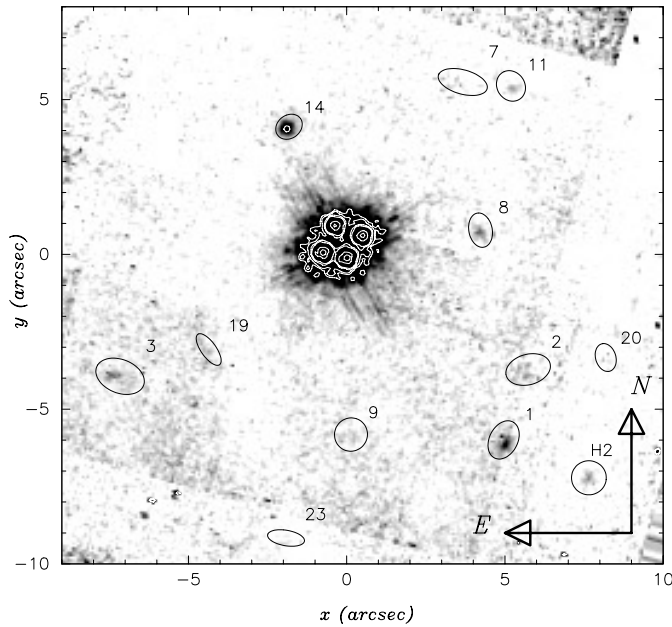


**Fig. 1.** Final NICMOS-2/F160W observation of the Cloverleaf. Ellipses indicate the objects detected in the WFPC2/F814W data (following the numbering of Kneib et al. 1998).

## 2. The HST/NICMOS-2 data

We retrieved the NICMOS-2/F160W observations of the Cloverleaf which do not hold proprietary rights (PI: E. Falco) from the STScI archive: <http://archive.stsci.edu/cgi-bin/hst>. The Cloverleaf data were taken on December 28, 1997 with a total exposure time of  $4 \times 640$  seconds. At the date of the observations, the NICMOS-2 pixel size ( $x, y$ ) was  $0.07603'' \times 0.07534''$  and the best PAM focus was at  $\sim 0.02$  (*c.f.* the NICMOS instrument WEB-page). The NICMOS data come in 3 different formats: raw (files \*\_raw.fits), calibrated (files \*\_cal.fits) and mosaiced (files \*\_mos.fits). The raw data set is made of 4 sets of 19 rasters. The calibrated data correspond to 4 flux calibrated frames, each being a combination of the 19 flat-field corrected images. We made our own mosaic of this dataset by combining the 4 flux calibrated frames shifted with non-integer number of pixels (Fig. 1). The image quality measured on the final mosaic is  $0.145''$  (FWHM).

The photometric calibration in the Vega system was determined from the PHOTNU FITS keyword following the NICMOS handbook recipe ( $\text{PHOTNU} = 2.3857 \times 10^{-6}$ ). The software SExtractor 1.2 (Bertin & Arnouts 1996) was used to detect and to derive the photometry of faint sources, with the detection parameters: 15 contiguous pixels over  $1.5\sigma$  of the sky-background after a convolution with a  $3 \times 3$  top-hat filter. Photometric properties and positions relative to quasar A of the different objects are summarized in Table 2.

## 3. The quadruple quasar and the primary galaxy-lens

In order to reveal the primary galaxy-lens amid the 4 quasar images, we have subtracted modeled PSFs of the NICMOS-2 cam-

**Table 1.** Relative positions (from Turnshek et al. 1997), photometry and flux ratios of the 4 quasar images relative to A (URI from Kneib et al. 1998, H this paper – magnitudes are given in the Vega system and not the WFPC2 system). Relative errors in U, R, I & H magnitudes are respectively  $\pm 0.02$ ,  $0.005$ ,  $0.005$  &  $0.02$ . Absolute errors on the magnitudes are typically  $\pm 0.1$ . Flux ratios Uncertainties are:  $\pm 4\%$  in U & H,  $\pm 1\%$  in R & I.

ID	$\Delta\alpha$ (")	$\Delta\delta$ (")	$U_{F336W}$ 94/12/23	$R_{F702W}$ 94/12/23	$I_{814W}$ 94/12/23	$H_{160W}$ 97/12/28
A	0.000	0.000	18.95	17.68	17.45	15.67
B	0.744	0.172	19.31 [0.73]	17.82[0.88]	17.58[0.89]	15.76[0.92]
C	-0.491	0.716	18.93 [1.01]	17.95[0.77]	17.73[0.76]	16.03[0.71]
D	0.355	1.043	19.13 [0.85]	17.97[0.74]	17.81[0.70]	16.29[0.57]

era. We used the TinyTim V4.4 software (Krist & Hook 1997) to model the NICMOS-2/F160W PSF over  $4 \times 4$  arcsec<sup>2</sup>. We set the instrument and telescope parameters to the values found in the FITS header and the NICMOS WEB page (PAM focus and cold mask position), and we assumed a flat spectrum for the quasar through the H160W filter. We oversampled the PSF with  $8 \times 8$  subpixels per NICMOS-2 pixel (in order to sample correctly the PSFs and position them accurately) and computed it at the 4 positions of the quasar images in each of the 4 calibrated frames. The positions of the 4 images of the Cloverleaf given in Turnshek et al. (1997) were used for the PSF subtraction (we also independently fitted the positions directly from the NICMOS image but it did not improve the subtraction), and the flux ratios were adjusted in order to minimize the weighted *mean* residuals at the 4 quasar images locations. This procedure was applied to each of the 4 calibrated frames, allowing us to derive the magnitudes and flux ratios of the 4 quasar images in  $H_{F160W}$  (Table 1), as well as independent errors on the photometry. We found some systematic residual patterns at each of the 4 PSF-subtracted quasar images, as expected in the case of a very complex PSF. We improved the PSF-subtraction by correcting the PSF from the *mean* value of the residual patterns measured at the 4 different quasar positions. A brightness excess amid the location of the 4 quasar images is conspicuous on each of the 4 calibrated frames, as shown on the final combined “quasar-free” image (Fig. 2). While there is no doubt about the detection of this source H1 (hereafter identified as the galaxy-lens), the signal-to-noise ratio prevents us to perform more sophisticated data processing.

In order to quantify the magnitude and position of the galaxy-lens, we have assumed that its profile follows a de Vaucouleurs law and included it in the fitting of the PSF subtraction. Parameters were chosen in order to be left, at this position, with a mean sky value similar to the median sky value. Fig. 2 shows the different steps in the subtraction procedure. Note that H1 is clearly detected *even* on the non-PSF subtracted image. Its position and  $H_{F160W}$  magnitude are given in Table 2. Unfortunately, we can only get lower limits to its  $R_{F702W}$  and  $I_{F814W}$  magnitudes, which prevents us from deriving a redshift constraint for H1.

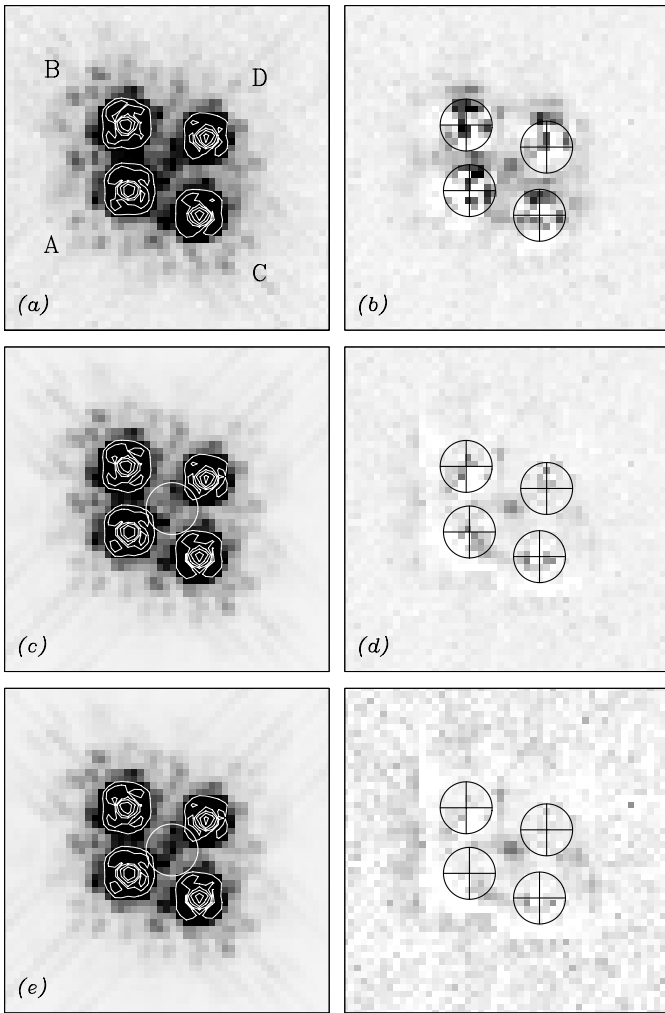


**Fig. 2a–f.** PSF subtraction steps (raster of  $3.7'' \times 3.7''$ ): **a** the NICMOS-2 data, **b** PSF subtraction of the 4 quasar images, **c** PSF model for the 4 quasar images, **d** PSF subtraction of the 4 quasar images corrected from the weighted mean of the 4 residuals in **b**, **e** PSF model for the 4 quasar images and the galaxy-lens, **f** same as **d** but normalized to the local noise (divided by the square root of the observed image). The orientation corresponds to the NICMOS-2 frame (PA of image from Y axis 74.38 degree).

In addition, we note that the quasar images flux ratios in H differ significantly from the ones in  $U_{F336W}$ ,  $R_{F702W}$  and  $I_{F814W}$ , particularly for D. As proposed by Turnshek et al. (1997), dust extinction can easily explain the different flux ratios. However microlensing on image D is also very likely (see Kayser et al. 1990), as it is the closest image to the detected galaxy-lens.

#### 4. Photometric redshifts of the faint objects surrounding the Cloverleaf

In the field-of-view covered by the  $H_{F160W}$  image, we identify 12 faint objects for which we can provide at least one of the  $R_{F702W}$ ,  $I_{F814W}$  or  $H_{F160W}$  magnitudes [in addition to H1]. Among these objects, 11 have been identified by Kneib

et al. (1998). Another one, called H2, was not detected either on the  $R_{F702W}$  or  $I_{F814W}$  images. All these objects are shown on Fig. 1. Their positions with respect to image A are given in Table 2, as well as their  $R_{F702W}$ ,  $I_{F814W}$  and  $H_{F160W}$  magnitudes.

We have estimated the redshift of these objects from their  $R_{F702W}$ ,  $I_{F814W}$  and  $H_{F160W}$  magnitudes, according to the standard minimization method described by Miralles & Pelló (1998). The updated Bruzual & Charlot evolutionary code (Bruzual & Charlot, 1993) was used and 5 different synthetic star-formation rates (SFR) tested: a 0.1 Gyr burst, a constant SFR, and 3  $\mu$  models (e-decaying SFR) with characteristic decay-time matching the sequence of colors for E, Sa and Sc galaxies. For each SFR type, 51 template spectra were selected with different stellar population ages. We also tested the stability of our results against different  $A_V$  values in the galaxies. The template database includes 255 solar metallicity spectra.

We have analyzed through simulations the accuracy and the possible biases affecting the redshift estimate from the photometry. For this purpose, a simulated catalogue of galaxies was created, with redshifts uniformly distributed between 0 and 6, and randomly sampling the SFR and ages. Photometric errors (uncorrelated for the different filters) were introduced as gaussian noise distributions with FWHM chosen so as to match the typical values for the Cloverleaf galaxy sample. According to these simulations, the use of the  $R_{F702W}$ ,  $I_{F814W}$  and  $H_{F160W}$  filters does not introduce any systematic bias in the redshift determination for  $0.5 < z < 2.5$ .

The most probable redshift was obtained for each object, as well as its probability (in the sense of  $\chi^2$ ) as a function of redshift (Table 2). We find that 9 objects have a redshift between 0.8 and 1.1, with  $\bar{z} = 0.9 \pm 0.1$ . Most of these objects are well fitted by a 1 to 2 Gyr burst model and  $A_V = 0$ . The  $I_{F814W}$  filter maps the B restframe at  $z \sim 0.9$ . The absolute magnitudes of these galaxies are  $-21 < M_B < -19$ .

For 4 objects (including the galaxy-lens H1 and the very red object H2) the redshift is poorly determined. The objects #14 and H2 are extremely red in  $(I_{F814W} - H_{F160W})$  and are consistent with galaxies at redshift 2 or higher. For object #14, the best-fit model (without reddening), is a 2.5 Gyr burst, which, given the redshift uncertainty, leads to  $M_B = -22.5$  to  $-23.9$ . This high luminosity suggests that object #14 might as well be gravitationally amplified by the cluster-lens with  $z \sim 1$ .

The photometric redshifts were computed using a solar metallicity. This is a fair approximation as, for  $1 < z < 2$  and the filters considered in this analysis, the results are not sensitive to metallicity. Furthermore, the estimated redshifts given in Table 2 are not sensitive to a reddening  $A_V < 2$ . Would be the reddening much higher, the estimated redshifts would shift toward lower values. However there is no reason to believe that all objects in the Cloverleaf field should be highly reddened. The dispersion is high, however, as reflected in the large interval at the 75% confidence level (Table 2); it is therefore important to effectively measure the redshift of the brightest objects to validate the current conclusion.

**Table 2.** Relative position (to quasar A), photometry and predicted redshift of the galaxies within  $10''$  of the Cloverleaf. The best matching redshift is given, as well as the permitted redshift interval corresponding to a 75% confidence level.

ID	$\Delta\alpha$ ('')	$\Delta\delta$ ('')	$I_{814W}$	$R_{F702W} - I_{814W}$	$H_{160W}$	$z_{\text{phot}}$ max	$\Delta z$ 75%	Comments
H1	0.112	0.503	>22.5	$R > 22.7$	$20.6 \pm 0.5$	–	–	the position accuracy is $\pm 0.02$ arcsec
H2	–7.6	–7.2	>24.8	$R > 25.5$	$21.6 \pm 0.7$	–	–	very red, only detected in H.
1	–7.3	–2.1	22.52	0.72	$20.7 \pm 0.3$	0.8	0.6–1.1	E/S0 morphology
2	–5.5	–3.7	23.11	0.86	$22.3 \pm 0.9$	0.9	0.8–1.0	
3	–0.6	8.2	23.16	0.88	$22.0 \pm 0.5$	0.9	0.8–1.0	disturbed morphology
7	3.9	–5.5	23.75	0.74	>22.3	0.9	0.5–1.2	
8	–0.7	–4.1	23.78	1.16	$21.8 \pm 0.5$	1.0	–	$z_{\text{phot}}$ solution at $\sim 50\%$ confidence level
9	–5.2	2.2	23.94	0.12	>22.3	–	–	no $z_{\text{phot}}$ constraint
11	3.2	–6.8	24.01	1.09	$22.3 \pm 0.8$	1.0	0.7–1.2	
14	4.7	0.2	24.37	>1.1	$20.0 \pm 0.2$	2.0	1.8–2.7	very red, possibly associated with absorbers
15	–2.2	–7.8	24.41	1.05	>22.3	0.8	0.6–1.2	
19	–0.9	5.3	24.74	0.88	>22.3	1.0	0.5–1.5	
20	–6.1	–6.1	24.78	>0.7	>22.3	1.1	0.2–1.6	$z_{\text{phot}}$ is poorly determined

## 5. Discussion and concluding remarks

Two main results have been obtained from the NICMOS-2 data. For the first time the galaxy-lens, H1, close to the line of sight toward the quasar, has been identified. Its position with respect to the quasar line-of-sight is found to be similar (within the uncertainties) to the one derived in the various Cloverleaf gravitational lens models (e.g. Kneib et al. 1998). A redshift estimate for H1 of  $\sim 1$  or higher is consistent with its  $H_{F160W}$  magnitude and its  $I_{F814W}$  lower limit. Clearly deep spectroscopic data are needed to solve for the determination of its redshift. Assuming that H1 belongs to the galaxy cluster at  $z \sim 1$ , and has colors and absolute magnitude similar to surrounding galaxies, we determine a mass-to-light ratio of  $M(< 5.1\text{kpc})/L_B \sim 25 M_{\odot}/L_{B\odot}$ .

We show that 8 nearby galaxies have a most probable redshift around 0.9, giving credit to the presence of a galaxy cluster/group along the line of sight to the Cloverleaf. In our previous modelling (Kneib et al. 1998), we assumed for this galaxy cluster/group a redshift of 1.7, as a mean of the redshifts of the 4 absorbers silhouetted on the quasar spectrum. This value should be revised. The location of the galaxy-lens is now known from the NICMOS-2 observations and will be implemented in a new model of the lens-system. One of the faint galaxies surrounding the Cloverleaf appears to be at a larger redshift, around 2, and might be related with the absorbers at  $z=2.07$  or  $2.09$  (Monier et al. 1998). Further imaging/spectroscopy of these galaxies should remove the remaining uncertainties of the Cloverleaf lens-system.

*Acknowledgements.* We would like to thank G. Bruzual for allowing the use of his code as well as for useful discussions on photometric redshifts. Many thanks to Jens Hjorth for a careful reading of this manuscript and fruitful discussions on lensing and other topics. DA wishes to thank Observatoire Midi-Pyrénées for hospitality.

## References

- Bertin, E., Arnouts, S. 1996, A&AS 117, 393  
 Bruzual, G., Charlot, S. 1993, ApJ 405, 538  
 Chartas, G., Chuss, D., Forman, W., Jones, C., Shapiro, I., 1998, ApJ, 504, 661  
 Hattori, M., Ikebe, L., Asaoka, I., et al, 1997, Nature 388, 146  
 Hjorth, J., Kneib, J.-P. 1998, ApJ submitted  
 Kayser, R., Surdej, J., Condon, J., et al. 1990, ApJ 364, 15  
 Keeton, C., Kochanek, C., Seljak, U. 1997, ApJ 482, 604  
 Kneib J.-P., Alloin D., Mellier Y., et al, 1998, A&A 329, 827  
 Krist, J. & Hook, R., 1997, The Tiny Tim User's Guide (<http://scivax.stsci.edu/krist/tinytim.html>)  
 Kundic, T., Turner, E., Colley, W., et al, 1997, ApJ 482, 75  
 Lawrence, C. 1996, in "Astrophysical Applications of Gravitational Lensing", eds. C. Kochanek & J. Hewitt, Kluwer, p. 209  
 Magain, P., Surdej, J., Swing, J.-P., et al, 1988, Nature 334, 325  
 Miralles J.-M., Pelló, R., 1998, ApJ submitted (astro-ph/9801062)  
 Monier, E., Turnshek, D., Lupie, O., 1998, ApJ 496, 177  
 Schechter P., Bailyn, C., Barr, R., et al, 1997, ApJL, 475, 85  
 Tonry J., 1998, AJ, 115, 1  
 Turnshek D., Foltz C., Grillmair C., Weyman R., 1988, ApJ 325, 651  
 Turnshek D., Lupie O., Rao S., Espey B., Sirola C., 1997, ApJ 485, 100